

# An Adaptive Walking Robot With Reconfigurable Mechanisms Using Shape Morphing Joints

Jiefeng Sun  and Jianguo Zhao , Member, IEEE

**Abstract**—In nature, animals or insects can leverage the same body parts for different functions (e.g., a frog can use its legs to walk, jump, and swim). But robots, especially miniature ones, can normally perform a single task with a fixed mechanical design. In this letter, we propose a novel strategy to enable reconfigurable robots by embedding shape morphing into a mechanism through shape morphing joints, which can be either soft for a compliant joint or rigid for a structure. In this case, a mechanism can achieve multiple trajectories without altering the mechanical design. We numerically analyze the reconfiguration strategy and apply it to a leg mechanism capable of generating different foot trajectories. With those trajectories, we implement the mechanism in a walking robot to demonstrate different functions. The proposed strategy can be leveraged to reconfigure other mechanisms to enable adaptive robots that can change their sizes, shapes, or functionalities to fulfill multiple tasks in different environments.

**Index Terms**—Biologically-inspired robots, legged robots, mechanism design, compliant joint/mechanism.

## I. INTRODUCTION

**I**N NATURE, animals or insects can leverage the same body parts to extend dynamic performance or achieve multiple functions [1]. For example, a bird can morph its wing to efficiently fly under different aerodynamic conditions. Frogs can use the same legs to jump, walk, and swim. Inspired by animals' superior adaptivity, roboticists have been exploring approaches to design reconfigurable robots that can adapt to various environments and tasks without altering its hardware design, especially mechanical parts. Such adaptive robots will have better stability, maneuverability, and energy efficiency than robots that only use their parts for a single task [2].

To adapt to different environments or functions, there are in general three different approaches. The first typical method uses multiple mechanisms or introduces several individually actuated degrees of freedom (DoFs) into a single mechanism. Multiple mechanisms in a single robot can enable robots with multimodal

Manuscript received September 10, 2018; accepted December 28, 2018. Date of publication January 16, 2019; date of current version February 4, 2019. This letter was recommended for publication by Associate Editor A. Ajoudani and Editor P. Rocco upon evaluation of the reviewers' comments. (*Corresponding author: Jiefeng Sun.*)

The authors are with the Department of Mechanical Engineering, Colorado State University, Fort Collins, CO 80523 USA (e-mail: J.Sun@colostate.edu; Jianguo.Zhao@colostate.edu).

This letter has supplementary downloadable material available at <http://ieeexplore.ieee.org>, provided by the author. The Supplemental Materials contain a video showing a novel strategy to enable reconfigurable robots by introducing into a mechanism with Shape Morphing joints (SMJs). This material is 17.2 MB in size.

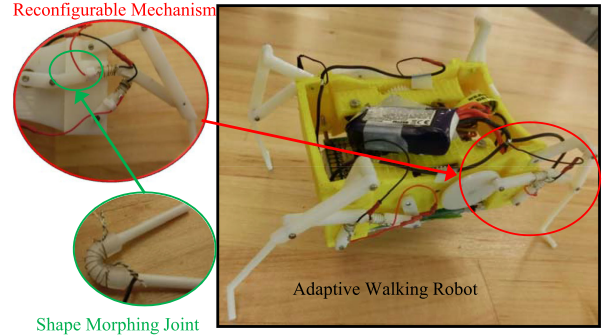


Fig. 1. An adaptive walking robot with reconfigurable mechanisms enabled by shape morphing joints (Video available at: <https://youtu.be/N2clvmSyqMc>).

locomotion. Examples include jumping robots with a tail for aerial maneuvering [3] or foldable wings for gliding [4]. Multiple DOFs in a single mechanism can coordinate the motion for each DOF to accomplish different trajectories. Examples include the well-known BigDog and the MIT Cheetah robot. The other two methods reconfigure the robot system passively or actively. The second method passively changes the robot's configuration using smart mechanical design (e.g., origami) to either negotiate obstacles [5] or withstand impact during collision [6]. The third method actively reconfigures underlying mechanical parts using additional actuators. For instance, linear actuators can change the link length in a linkage to generate efficient locomotion that mimics different animal species [7], [8], or help to adapt to varying ground conditions [9].

Generally, additional actuators used in the third method are motors, but tendons [10], pneumatic actuators [11] and smart materials such as shape memory alloy [12] or twisted-and-coiled actuators [13] have also been used to form a compact shape morphing system. Because most of these smart materials are not rigid enough, variable stiffness elements [14] such as shape memory polymers [15], low-melting point alloys (LMPA) [16], or thermoplastics [13], [17] are introduced to hold the new reconfiguration.

In general, however, existing approaches are not suitable to accomplish multiple functions for miniature centimeter-scale robots. The small size and weight prevent us from using multiple mechanisms or many actuators. Although the passive approach does not require any additional component, it has a limited reconfigurability. Therefore, we need to find new approaches for adaptive and miniature robots.

In this letter, we propose a new reconfiguration strategy by introducing into a mechanism with shape morphing joints (SMJs),

which can be either soft for a compliant joint or rigid for a structure. With several SMJs in a mechanism, we can change its functionality by strategically softening and solidifying appropriate SMJs, without altering the underlying mechanical design after it is fabricated. Further, we use the same motor that drives the mechanism to transform it to other configurations. Potentially, reconfigurable mechanisms with SMJs can enable adaptive robots that can adjust their sizes, shapes, or functions to fulfill multiple tasks in different environments. The general concept proposed in this letter is shown in Fig. 1.

The main contribution of this letter is a new reconfigurable strategy by embedding SMJs into mechanical mechanisms. The strategy can be potentially applied to other mechanisms to generate different configurations or trajectories. Such a strategy will also provide a new perspective for other areas such as shape morphing structures, metamorphic mechanisms, deployable structures, or programmable matter. In addition to this main contribution, we numerically analyze the reconfiguration strategy for a fundamental mechanism with two SMJs, which can guide the reconfiguration for other mechanisms. We also apply the strategy to analyze the transition between three example trajectories of a specific mechanism for walking robots.

The rest of this letter is organized as follows. In Section II, we introduce the working principle, fabrication, and characterization of SMJs. In Section III, we present a fundamental reconfigurable mechanism with two SMJs, and analyze the usable range of the reconfiguration. We also theoretically model the trajectory before and after reconfiguration using a pseudo-rigid-body model, and experimentally verify the modeling results. In Section IV, we implement the fundamental mechanism in the first loop of a Klann walking mechanism to demonstrate the reconfiguration. The Klann mechanism is applied to a miniature walking robot, demonstrating its capability to avoid overhead obstacles.

## II. SHAPE MORPHING JOINTS (SMJs)

Soft joints or compliant joints, formed by soft or flexible materials instead of bearings and shafts, are usually used in compliant mechanisms [18]. They are similar to conventional revolute joints except that they cannot rotate in a full revolution. However, most of existing compliant joints have a fixed stiffness, resulting in a fixed behavior for mechanisms having those joints. With recent advances in stiffness controllable materials such as thermoplastics [19] and LMPAs [16], it would be interesting to see how we can enable an SMJ using those materials, and then use SMJs to morph the shape of links to reconfigure a given mechanism.

### A. Design and Fabrication of SMJs

Our proposed SMJ is made of three components as shown in Fig. 2(a). First, the key element is the stiffness controllable material. Although many choices are available, we choose polylactide (PLA), a thermoplastic material used for 3D printing, because of its low-cost and low glass transition temperature ( $T_g$ ). For PLA, the stiffness drastically decreases if its temperature is above  $T_g \approx 62^\circ\text{C}$ . Second, we use a soft silicone tube to enclose the PLA to ensure that the resulting SMJ can still

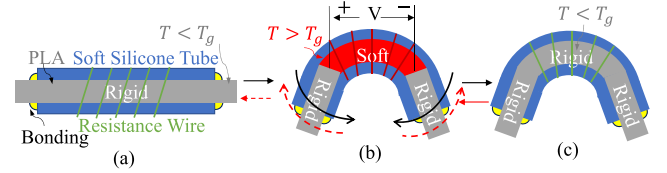


Fig. 2. Schematic of the SMJ.

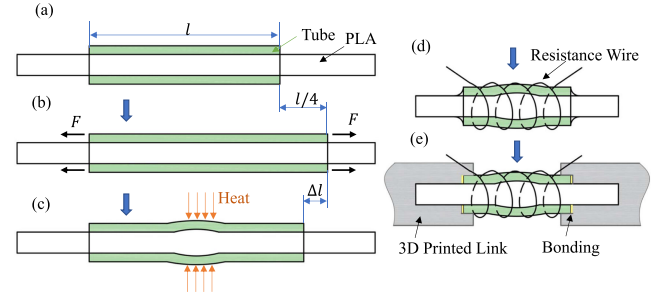


Fig. 3. SMJ fabrication process, showing details of the joint.

support external loads even when the PLA inside becomes very soft. Third, we wrap some resistance wire around the tube for Joule heating to increase the SMJ's temperature. We also bond the tube and the PLA with glue at both ends to make the joint more robust.

Such an SMJ will function as follows (Fig. 2 and Supporting Video). Initially, the SMJ is rigid (Fig. 2(a)). When the PLA is heated above its  $T_g$  (Fig. 2(b)), it softens and the SMJ becomes a soft joint to freely rotate. Then we can rotate it to a desired angle and stop heating the PLA. After cooling down, the SMJ will become rigid to hold the new shape (Fig. 2(c)). If reheated, it becomes a soft joint again and can return to the original shape if a moment is applied (Fig. 2(b) to 2(a)).

The proposed SMJ is fabricated in the following steps as shown in Fig. 3. A PLA printing filament with a diameter of 1.75 mm is straightened by slightly stretching it under a heating gun. First, the straight PLA rod is inserted into a  $l = 16$  mm long silicone tube (Sani-Tech, ULTRA-C-062-1) with an inner diameter of 1.6 mm and a wall thickness of 0.8 mm. Second, we stretch the tube 25% and the friction between the tube and the PLA rod will keep the tension of the tube. Third, we heat the assembly (tube and PLA) with a heating gun (set at  $120^\circ\text{C}$ ) until the length of the tube does not change so that the tube will drag the PLA to include more PLA inside. Such a procedure can ensure the PLA will not break up after many rotations. Fourth, we cut the tube to a length of 9 mm and wrap a 7 mm long resistance wire (UXCELL Nichrome, diameter 0.1 mm) on the outer surface of tube uniformly to form a 7 mm long heating section. The resistance wire is insulated before the wrapping process with Rotanium Insulation Spray to prevent the change of resistance when neighboring coils contact. Two copper wires anchored at the two ends of the resistance wire serve as leads to apply electricity. The final resistance of the SMJ is  $9\ \Omega$ . Also, a small amount of super glue gel is applied to the ends of the tube to bond the PLA rod and the silicone tube. We can integrate an SMJ into a link of a mechanism to enable reconfigurable mechanisms to be discussed in Section III-D. Towards this goal,

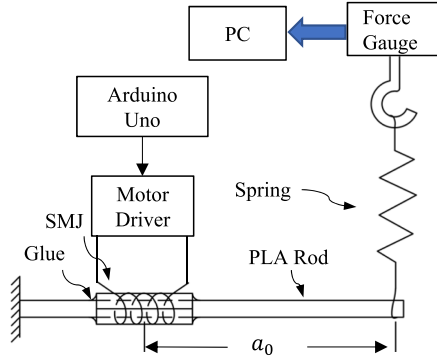


Fig. 4. Experimental setup for SMJ characterization.

we can cut the PLA rod and the tube of the SMJ to 15 mm and 9 mm separately, as shown in Fig. 3(d). Then both ends of the PLA rod are inserted into the holes of rigid links (Fig. 3(e)) that are 3D printed by an OJBET30 PRO printer (Stratasys Inc.) with VeroWhitePlus material. Then additional glue is applied to bond the tube to the countersinks of the links.

#### B. Characterization of SMJs

For untethered robots, we can maximize their operation time by minimizing energy consumption. Therefore, we need to minimize the input power to soften a SMJ by maintaining the PLA's temperature slightly over  $T_g$ . However, it's difficult to measure the PLA's temperature since it is complicated to place a temperature sensor inside the SMJ due to its small size. Therefore, we experimentally find the minimal power by using the stiffness of the SMJ to indicate the temperature inside.

For such an experiment, we apply different but constant input voltages and use an external force sensor to determine when will the SMJ becomes soft. To better visualize the result, we apply a constant pretension force at the end of the SMJ using a linear spring. Once the PLA rod in the SMJ reaches its  $T_g$ , its stiffness will be negligible and the final tension force in the spring will be the balanced force ( $F_b$ ) between the spring and the soft tube. By observing the tension force from the force sensor, we can identify the optimal power input: the smallest power that allows the force in the spring to drop to  $F_b$ .

According to the principle above, the experimental setup is shown in Fig. 4. A linear spring (an elastic rubber band with a stiffness of  $k = 12 \text{ mN/mm}$ ) pulls the SMJ with a moment arm of  $a_0 = 20 \text{ mm}$ . The pretension force along the spring is set to 60 mN by adjusting the location of a force gauge (Mark-10-M3-012, precision 0.5 mN) attached at the other end of the spring. The pretension force 60 mN is experimentally found since a larger value may cause excessive initial bending of the SMJ and a smaller one might induce a large error based on the precision of the force gauge. The force gauge is connected to a computer to sample data at 5 Hz. A motor driver (Pololu, DRV8835) controlled by an Arduino board applies electricity to the SMJ.

The balanced force  $F_b$  is experimentally obtained by replacing the PLA in the SMJ section with water to obtain a soft joint. We first fix the soft joint in a straight shape and pull it using the

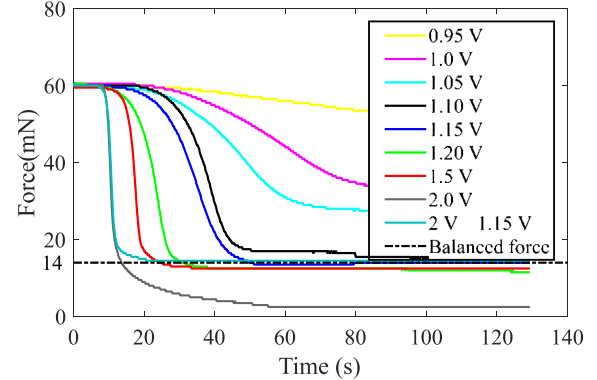


Fig. 5. SMJ Characterization.

spring and the force gauge with 60 mN. Then we release the soft joint and let it balance with the spring. The steady-state force of the force gauge is 14 mN.

Different constant voltages starting from 0.95 V to 1.20 V with a step size of 0.05 V are used to heat up the joint from room temperature. The tension force corresponding to different voltages are plotted in Fig. 5. From the figure, when the voltage is 1.15 V, the measured tension force after 50 s is approximately 14 mN. Therefore, the corresponding power 0.145 W is the optimal power input. When the input is much larger (e.g., 2.0 V), the steady-state tension force drops below 14 mN, probably due to the change of the stiffness of the tube, suggesting a larger input voltage is undesirable.

To reduce the time for softening a SMJ, we can first apply a higher power to soften the joint and then input the optimal power to maintain the softness. So, we experimentally find a two-step heating strategy: first heat the SMJ with an input of 2 V for 11 s, the time that the measured force drops to 14 mN, and then reduce the input to 1.15 V. The measured force for this strategy is also shown in Fig. 5, indicating the required heating time is significantly reduced from 50 s to 11 s.

### III. THE FUNDAMENTAL RECONFIGURABLE MECHANISM WITH SMJs

If we incorporate SMJs into mechanical linkages, several new interesting phenomena emerge. To illustrate them, we will use an example setup (Fig. 6(a)) with three traditional revolute joints and two ideal SMJs, with rotational axis at the SMJ's center. The three traditional revolute joints are located at  $A$ ,  $B$ , and  $D$ , and two SMJs are located at  $C_1$  and  $C_2$ . With this simple setup, we have two interesting observations. First, SMJs can enable both rigid structures and movable mechanisms. If both  $C_1$  and  $C_2$  are rigid, then the setup is a rigid structure since it only has three revolute joints. If only one SMJ is soft, then the setup is a four-bar linkage, which will have different trajectories based on the choice of  $C_1$  and  $C_2$ . Further, if both SMJs are soft, the setup will be a five-bar linkage. Second, we can also reconfigure the setup's geometry by sequentially softening and solidifying  $C_1$  and  $C_2$ . For example, we can first soften  $C_2$  to move the four-bar linkage to a specific configuration. After that, we can

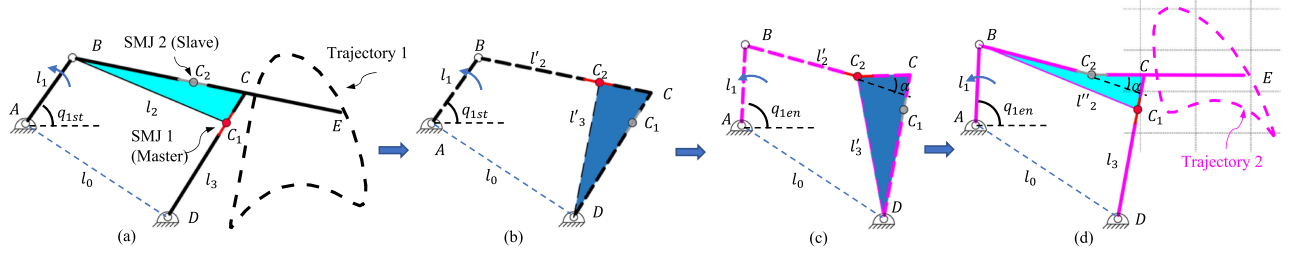


Fig. 6. Schematic of the fundamental reconfigurable mechanism.

solidify  $C_2$  and then soften  $C_1$ . In this case, the effective link length  $BC_1$  will change, altering the configuration of the setup.

The second observation can generate different trajectories for multiple functions. In the following, we will use the setup in Fig. 6(a) as a fundamental mechanism to illustrate and analyze the reconfiguration strategy. Potentially, this fundamental mechanism and the reconfiguration strategy can be included into other more complicated mechanisms that have multiple closed loops for reconfiguration purposes such as the Watt II, Stephenson II and III linkages.

#### A. Reconfiguration Strategies and Nomenclatures

As shown in Fig. 6, the thick solid line (or the dash line in b and c) represents the mechanism with four links  $AB$ ,  $BCE$ ,  $CD$ , and  $DA$ , where  $AB$  is the drive link. We are interested in generating different trajectories for point  $E$  by reconfiguring the fundamental mechanism.

To better illustrate the reconfiguration strategies, we name one SMJ in the mechanism as a ‘master’ joint and the other a ‘slave’ joint. The master joint will serve as a soft joint before and after the reconfiguration process to enable a four bar linkage. The slave joint only becomes a soft joint in the reconfiguration process. Any SMJ can be either a slave or a master joint depending on different tasks.

Here, as an example, we study the case when  $C_2$  works as a slave joint and  $C_1$  as a master joint, and discuss the reconfiguration process as shown in Fig. 6. Before the reconfiguration, the mechanism generates trajectory 1 when  $C_2$  is rigid (shown in gray color) and  $C_1$  works as a soft joint (shown in red color), as shown in Fig. 6(a), where the shaded area  $BCC_1$  is a rigid link. In the reconfiguration process,  $C_1$  becomes rigid and  $C_2$  works as a soft joint (Fig. 6(b)). Link  $AB$  will rotate to morph the shape of the link  $BC_2C$ , i.e., bend the original straight link  $BC$  into an angle  $\alpha$  at  $C_2$  (Fig. 6(c)). After the reconfiguration (Fig. 6(d)),  $C_2$  becomes rigid to fix link  $BC_2C$  in a bent shape, and  $C_1$  serves as a soft joint again to allow the mechanism to generate a different trajectory 2.

Different trajectories are generated because the effective length  $BC_1$  changes after the reconfiguration (Note the difference for  $BC_1$  in Fig. 6a and 6(d)). The altered length of  $BC_1$  is uniquely determined by the bent angle  $\alpha$  of link  $BC_2C$ . Therefore, we need to investigate the range of  $\alpha$ .

Toward this goal, we have the following definitions to facilitate discussions. First, we say an angle  $\alpha$  is *available* if it can be achieved in the morphing process. Second, since we will

use the fundamental mechanism for a walking mechanism in Section IV, we are interested in the case when the drive link can rotate in a full revolution. Therefore, we further classify the available  $\alpha$  into two types: *usable* and *unusable*, with usable  $\alpha$  allowing the drive link to rotate in a full revolution. Third, to achieve a desired  $\alpha$ , we need to appropriately choose the starting angle  $q_{1st}$  and the ending angle  $q_{1en}$  for the drive link  $AB$  during the reconfiguration process (Fig. 6(b) and 6(c)). We call  $q_{1st}$  and  $q_{1en}$  a reconfiguration angle pair (RAP).

#### B. Analysis of Reconfiguration Strategies

To achieve a configuration that can generate a desired trajectory for point  $E$ , we need to find a reconfiguration strategy (i.e., find a RAP) to achieve a given  $\alpha$ . Towards this goal, we first try to analyze the reconfiguration process to find the available range of  $q_{1en}$  in terms of  $q_{1st}$  as well as analyze the available and usable range of  $\alpha$ . Since the drive link  $AB$  will rotate a full cycle and the other links only swing, we choose  $q_{1st}$  and  $q_{1en}$  to be in  $[0, 2\pi]$  and  $\alpha$  to be in  $[-\pi, \pi]$ . In the following analysis, we assume that all the SMJs are ideal ones that rotate around their centers. Also, without loss of generality, we assume the following dimensions for the link length:  $|AB| = 10.3$  mm,  $|BC_1| = 19.5$  mm,  $|C_2C| = 8.3$  mm,  $|CC_1| = 5$  mm,  $|CD| = 14.6$  mm, and  $|CE| = 18$  mm.

First, the  $q_{1en}$  will depend on a given  $q_{1st}$ . Therefore, we define a loop usable indicator to identify the range of  $q_{1st}$  that will allow link  $AB$  to rotate a full revolution during the reconfiguration process:

$$\delta_1(q_{1st}) = l'_2 + l'_3(q_{1st}) - (l_1 + l_0) \quad (1)$$

where  $l_0$ ,  $l_1$ ,  $l'_2$  and  $l'_3(q_{1st})$  are link lengths for link  $AD$ , link  $AB$ , link  $BC_2$  and link  $C_2D$  shown in Fig. 6(b) and  $l'_3(q_{1st})$  is a function of  $q_{1st}$ . Based on such a definition, we can solve  $\delta_1$  in terms of  $q_{1st}$ . When  $q_{1st} \in [0.43\pi, 1.27\pi]$ , drive link  $AB$  can rotate in a full revolution, meaning  $q_{1en}$  can be any value. If  $q_{1st} \notin [0.43\pi, 1.27\pi]$ , we can only choose a  $q_{1en}$  from a limited range.

After that, we can plot  $q_{1en}$  in terms of  $q_{1st}$  (Fig. 7) by solving extreme configurations that the distance between point  $B$  and  $D$  ( $l_{BD}(q_{1en})$ ) reaches its maximum possible length, which is  $l_{BD}(q_{1en}) = l'_2 + l'_3(q_{1st})$ . We can see that when  $q_{1st}$  is in  $[0, 0.43\pi]$  and  $[0.43\pi, 1.27\pi]$ , there are unavailable domains for the RAPs shown as the blank areas. Also, to avoid going through singularity configuration that the point  $C_2$  is below the  $AD$  line, we restrain link  $AB$  to rotate counterclockwise in the reconfiguration process, resulting in an unusable domain shown

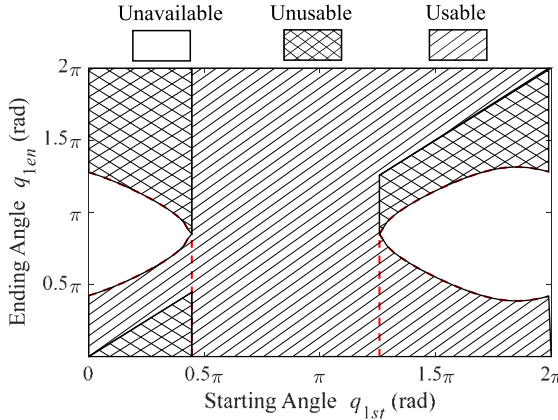


Fig. 7. Different regions for reconfiguration illustrated using the ending angle  $q_{1en}$  with respect to  $q_{1st}$ .

in Fig. 7. However, as long as we choose a proper RAP in the usable domain, we may still achieve a desired  $\alpha$ .

Then we need to investigate if it is possible to achieve a given  $\alpha$ . There might be multiple RAPs for a given  $\alpha$  since  $\alpha$  is essentially a joint variable that continuously changes in the reconfiguration process. To find the usable range, we define another usable indicator after the reconfiguration

$$\delta_2(\alpha) = l''_2(\alpha) + l_3 - (l_1 + l_0) \quad (2)$$

where  $l''_2(\alpha)$  and  $l_3$  are link lengths for link  $BC_1$  and link  $C_1D$  shown in Fig. 6(d).  $l''_2(\alpha)$  is a function of  $\alpha$ , and  $\alpha = f(q_{1st}, q_{1en})$  is a function of the RAP, which depends on the reconfiguration process. Under the requirement  $\delta_2(\alpha) > 0$ , we can numerically solve the usable range of  $\alpha$  as  $[0, 0.43\pi]$ , of which the boundary values are obtained using  $\delta_2(\alpha) = 0$ .

Note that the usable range of  $\alpha$  is a subset of its available range. Therefore, if a desired  $\alpha$  is within the usable range, we can directly solve the geometry to find the RAP using position analysis methods such as closed-form equations and complex number method [20].

### C. Pseudo Rigid Body Model for SMJs

In the previous analysis, we assume the SMJs are ideal revolute joints with a fixed rotational axis at the center to explain the properties of the reconfiguration strategy. However, this ‘ideal shape morphing joint’ model is accurate only when the length of the SMJ is really small compared with the size of the mechanism [18].

When a compliant joint behaves like a bending beam instead of a revolute joint, the rotation axis will vary with force and moments applied to the joint, influencing the trajectory of the mechanism. Various models on kinematics and even dynamics of compliant mechanisms have been proposed to solve the problem. For example, finite element analysis (FEA) tends to be highly accurate, but time-consuming and computationally expensive. The most widely-used, simpler models are the pseudo rigid body models (PRBM) such as 1R model [21], 3R model [22], and RPR model [23].

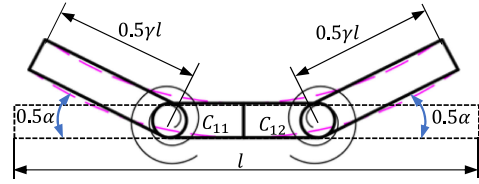


Fig. 8. Pseudo rigid body 1R model for the SMJ.

Here we use the classical 1R model to model an SMJ in the soft state and verify the model in the next subsection by experimentally comparing trajectories of point E in the mechanism. The usable range described in Section III-B can be analyzed similarly by replacing the ideal revolute joint model with the 1R model.

PRBM 1R model approximates the large nonlinear deflection of a cantilever beam with two rigid links connected with one revolute joint. An SMJ can be treated as a combination of two 1R models: 3 rigid links connected by two ideal revolute joints with one torsional spring in each joint (Fig. 8).  $\gamma$  is the characteristic radius factor and determines the location of the instantaneous center for rotation. Although  $\gamma$  generally varies with respect to different loads ratios between forces and moments, an averaged value can be found through optimization to minimize the modeling error. We will simply use the average value  $\gamma_{ave} = 0.85$  [18] to model the SMJ. With  $\gamma_{ave}$ , we can use a vector loop equation to solve all joint angles to simulate the trajectory of point E [20].

### D. Experimental Results for the Fundamental Mechanism

We fabricate the fundamental reconfigurable mechanism using the technique described in Section II-A. The dimensions are the same as presented in Section III-B, except that  $BC_2$  and  $DC_1$  are measured from the center of the SMJs when the SMJs are straight and that we set an  $\pi/8$  angle between  $BC$  and  $CE$ . The final lengths of the SMJ1 and SMJ2 are 6 mm and 7 mm. The other conventional revolute joints use small screws (M1.2 × 6) as shafts.

The mechanism is driven by a motor (Pololu, 6V-MP-75:1) with an encoder, of which the rotational speed and position can be precisely controlled by an Arduino Uno board. Voltages are applied to SMJs with a motor driver (Pololu, DRV8835) controlled by the same Arduino Uno board. We record the different trajectories of point E by placing a camera right in front of the mechanism. Tracker software ([physlets.org/tracker](http://physlets.org/tracker)) is used to obtain the trajectory data. We choose  $q_{1st} = 0$  and  $q_{1en} = 85^\circ$  and the detailed reconfiguration sequence of the platform will be introduced later in IV-B. Fig. 9 shows the simulated trajectories using 1R model and experimental trajectories for point E before and after the reconfiguration, respectively.

An error analysis is performed to quantify the accuracy of the method. The equation used to calculate this error is:  $error = \sqrt{(X_{exp} - X_{model})^2 + (Y_{exp} - Y_{model})^2}$ . We find that the average error is 0.82 mm for 1R model and, as a comparison, 1.96 mm for the ideal revolute joint model. The reasons why the 1R model cannot give higher accuracy are the linear extension

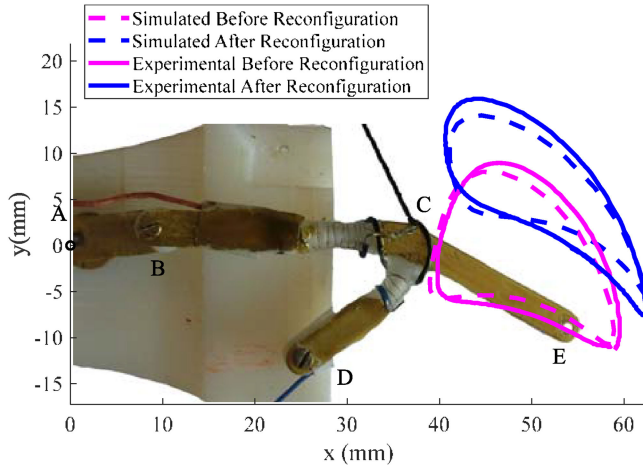


Fig. 9. Comparisons of experimental and simulated trajectories for point E.

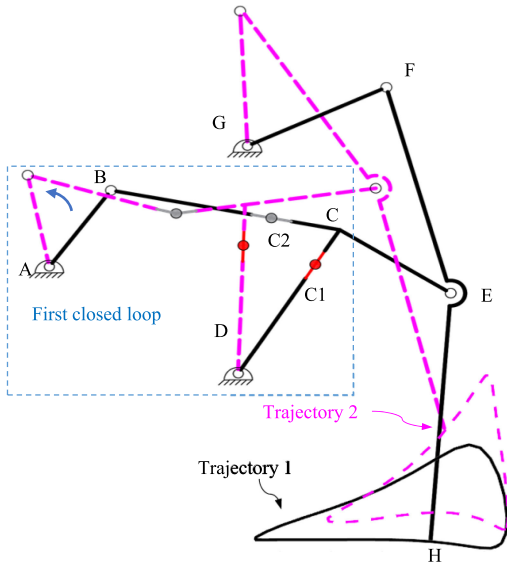


Fig. 10. Schematic of the reconfigurable Klann mechanism.

of the SMJs and the fabrication error. However, we can still conclude that the 1R model provides a better match with the experimental results. More complicated models such as FEA, 3R and RPR model might be applied to get better results.

#### IV. ADAPTIVE WALKING ROBOT

The fundamental reconfigurable mechanism can serve as a basic loop in more complicated mechanisms with multiple loops. A typical example is the Klann mechanism [24], which has been widely used for walking robots since it can generate biomimetic foot trajectories [25]. In this section, we will illustrate the reconfiguration for the Klann mechanism to generate different foot trajectories.

The structure of a Klann mechanism with SMJs is shown in Fig. 10. It has the fundamental reconfigurable mechanism as the first closed loop, the end of which is connected to another loop with three traditional revolute joints. If only one SMJ is soft, the mechanism will have one DOF. In Fig. 10, we have plotted two

different trajectories that can be generated by reconfiguring the first closed loop according to strategies discussed in Section III.

##### A. The Reconfigurable Klann Mechanism

To fabricate the reconfigurable Klann mechanism, we assemble the normal links that printed with OJBET 30 printer and the links fabricated in Fig. 3. The designed links for the first closed loop have the same dimensions as the fundamental reconfigurable mechanism, but two more links are added ( $|GF| = 21$  mm,  $|EF| = 30$  mm,  $|EH| = 35$  mm and the angle between  $EF$  and  $EH$  is  $\pi/18$ ). These dimensions are mainly based on our previous work [25]. With these SMJs and the strategy presented below, the reconfigurable Klann mechanism can change its reconfiguration to achieve multiple tasks, significantly enhancing its capability.

##### B. Reconfiguration Between Three Trajectories

Through the strategy discussed in Section III, we reconfigure the mechanism to generate three trajectories. First, a normal walking trajectory is generated when  $C_1$  is the master joint. Second, an obstacle avoiding trajectory is generated to allow the robot to lower its body and avoid overhead obstacles. Third, a trajectory that can be potentially used for jumping is created by using  $C_2$  as the master joint and  $C_1$  as the slave joint. Also, different jumping trajectories can be obtained through a similar reconfiguration process to bend the link where the new slave joint ( $C_1$ ) locates.

Fig. 11 shows the reconfiguration from the normal walking trajectory to the obstacle avoiding trajectory through the following process: (a) the mechanism generates a normal walking trajectory with SMJ 1 (master joint labeled with a solid red circle) as a soft joint, and SMJ 2 (slave joint labeled with a solid gray circle) is rigid; (b) the mechanism stops when the drive link is in 0 angle and SMJ 2 is heated over its glass transition temperature while SMJ 1 is cold and rigid; (c) the motor rotates to  $85^\circ$  to make SMJ 2 to deform to a specific angle; (d) cool down the deformed SMJ 2 and heat up SMJ 1; (e) the mechanism can generate the new obstacle avoiding trajectory with SMJ 1 as a soft joint. The time sequence for the actuation of motors and SMJs is shown in Fig. 12.

The three foot trajectories are also obtained and plotted in Fig. 13 from videos using Tracker. From the figure, the flat portion of the obstacle avoiding trajectory is raised for 8.5 mm from the normal walking trajectory. It means that the robot with this trajectory can lower its height 8.5 mm to avoid overhead obstacles so that it can go through a clearance that it previously cannot. The jumping trajectory is along a single line, which is drastically different from the two walking trajectories.

##### C. Reconfiguration of the Adaptive Walking Robot

We build an untethered walking robot with four Klann mechanisms to demonstrate that the reconfigurable mechanism can make the robot adapt to its environment. The robot is actuated only by two motors so that it can turn. Further, since the reconfiguration does not require additional motors, it has a compact

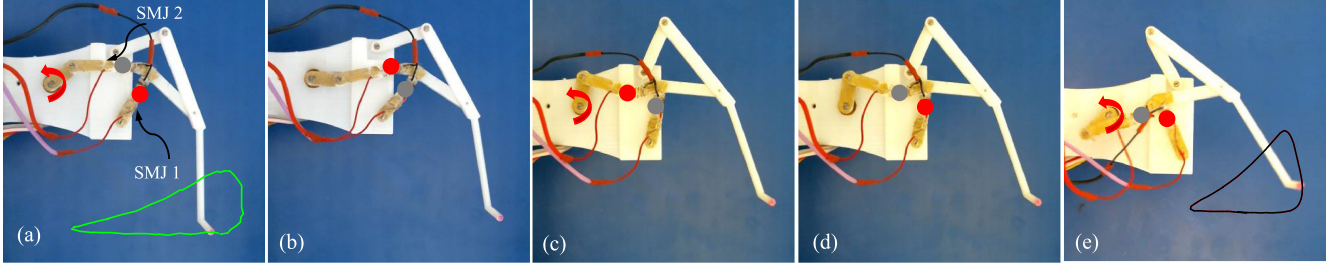


Fig. 11. The transition from a normal walking trajectory to an obstacle avoiding trajectory.

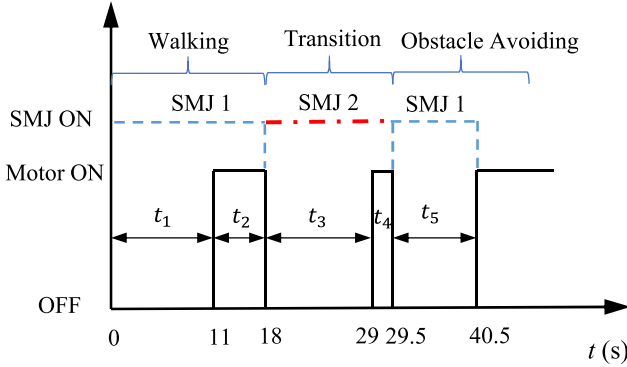


Fig. 12. The actuation sequence of the motor and SMJ.

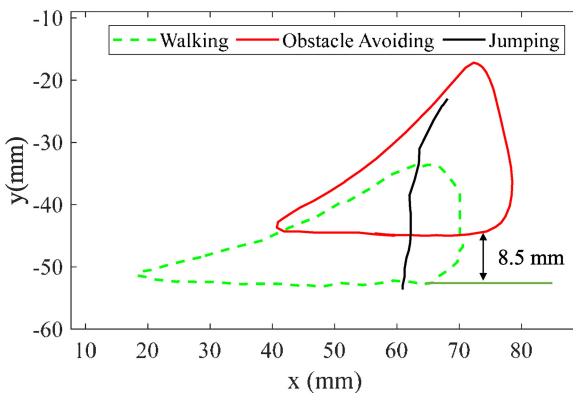


Fig. 13. Experimental results for the three trajectories.

size (dimension:  $15 \times 10 \times 8$  cm), and to the best of our knowledge, it is the smallest, motor-actuated, reversibly reconfigurable quadruped robots.

The robot base is 3D printed using Lulzbot Mini printer. The two motors are the same types of motor used in the single leg platform. The two Klann mechanisms on the same side are actuated by one motor through gear transmissions. A customized control board is developed to control the actuation sequence of motors and SMJ. Before walking, the robot is preset at an amble walking pattern with the four legs at 0, 0.75, 0.25, 0.5 of its cycle [26]. The robot weighs 113 g including a 7.4 V rechargeable LiPo battery.

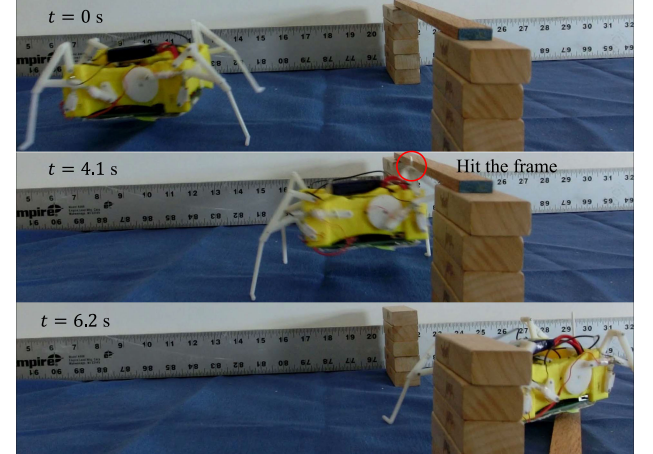


Fig. 14. Sequential images showing the robot hits the frame with a normal walking trajectory.

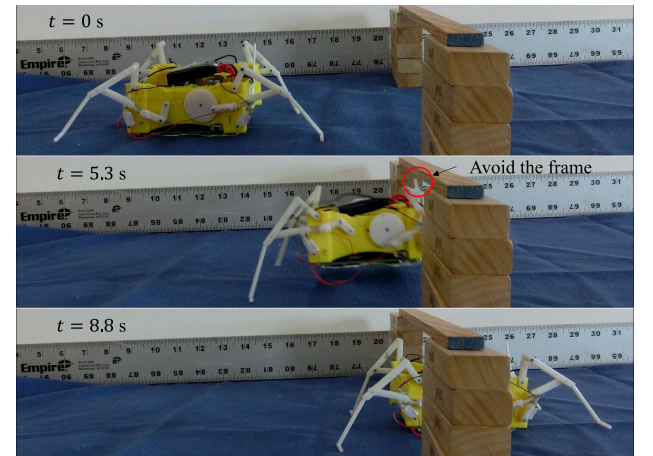


Fig. 15. Sequential images showing the robot avoids the frame after reconfiguration.

We demonstrate that the robot can walk through the bottom of an artificial ‘door’ by lowering its height. Fig. 14 shows the robot can walk on a flat ground using the normal walking trajectory, but it will hit the obstacle (see Supporting Video). After reconfiguration, as shown in Fig. 15, the robot can lower its body to avoid the obstacles and successfully go through the door. We leave the demonstration of the jumping trajectory as future work since the current robot is too heavy for jumping.

The robot shows wobbling walking because it can only touch the ground with two legs at any moment since two legs at the same side are actuated by a single motor to reduce the number of actuators. As a result, the balancing of our robot only relies on a passive dynamic stability. The problem can be fixed by actuating each leg with an independent motor, so that a coordinated motion will allow for three of the four legs touching the ground all the time.

## V. CONCLUSIONS

In this letter, we propose the concept of reconfigurable mechanisms with shape morphing joints. Such mechanisms can change its motion trajectory by morphing the shape/length of its links. Experiments are conducted to find the optimal voltage that can keep the SMJ soft with minimum energy input. We discuss the reconfiguration process and usable solutions for a given reconfiguration task using a fundamental reconfigurable mechanism. We leverage a pseudo-rigid-body model for SMJs to predict the trajectory for the mechanism. We also build a reconfigurable Klann mechanism with the fundamental mechanism to demonstrate the transition between different trajectories. An adaptive walking robot using four reconfigurable Klann mechanisms is also developed. The robot can walk on the flat ground and reconfigure to avoid overhead obstacles. We anticipate that the proposed concept in this letter can realize multifunctional robots without altering their mechanical design.

Although the proposed reconfiguration strategy can change the motion of a given mechanism effectively, two potential issues require further research. First, the reconfiguration time is currently relative long, requiring 22.5 s in total to morph the mechanism to generate two trajectories. Such a problem can be potentially solved by using other stiffness controllable materials such as LMPAs or Polymorph as well as exploring different geometries for the joint. Second, we still need to develop more precise models to predict the reconfiguration process when external loads exist. This issue can be addressed by leveraging more sophisticated theories from compliant mechanisms.

## REFERENCES

- [1] E. Muybridge, *Animals in Motion*. North Chelmsford, MA, USA: Courier Corp., 2012.
- [2] S. Mintchev and D. Floreano, "Adaptive morphology: A design principle for multimodal and multifunctional robots," *IEEE Robot. Autom. Mag.*, vol. 23, no. 3, pp. 42–54, Sep. 2016.
- [3] J. Zhao, T. Zhao, N. Xi, M. W. Mutka, and L. Xiao, "MSU tailbot: Controlling aerial maneuver of a miniature-tailed jumping robot," *IEEE/ASME Trans. Mechatronics*, vol. 20, no. 6, pp. 2903–2914, Dec. 2015.
- [4] M. A. Woodward and M. Sitti, "Multimo-bot: A biologically inspired integrated jumping–gliding robot," *Int. J. Robot. Res.*, vol. 33, no. 12, pp. 1511–1529, 2014.
- [5] Y.-S. Kim, G.-P. Jung, H. Kim, K.-J. Cho, and C.-N. Chu, "Wheel transformer: A wheel-leg hybrid robot with passive transformable wheels," *IEEE Trans. Robot.*, vol. 30, no. 6, pp. 1487–1498, Dec. 2014.
- [6] S. Mintchev, J. Shintake, and D. Floreano, "Bioinspired dual-stiffness origami," *Sci. Robot.*, vol. 3, no. 20, 2018, Art. no. eaau0275.
- [7] S. Nansai, N. Rojas, M. R. Elara, and R. Sosa, "Exploration of adaptive gait patterns with a reconfigurable linkage mechanism," in *Proc. IEEE/RSJ Int. Conf. Intell. Robots Syst.*, 2013, pp. 4661–4668.
- [8] J. K. Sheba, M. R. Elara, E. Martínez-García, and L. Tan-Phuc, "Synthesizing reconfigurable foot traces using a Klann mechanism," *Robotica*, vol. 35, no. 1, pp. 189–205, 2017.
- [9] F. I. Sheikh and R. Pfeifer, "Adaptive locomotion on varying ground conditions via a reconfigurable leg length hopper," in *Adaptive Mobile Robotics*. Singapore: World Scientific, 2012, pp. 527–535.
- [10] A. Firouzeh, M. Salerno, and J. Paik, "Stiffness control with shape memory polymer in underactuated robotic origamis," *IEEE Trans. Robot.*, vol. 33, no. 4, pp. 765–777, Aug. 2017.
- [11] W. Shan, S. Diller, A. Tutcuoglu, and C. Majidi, "Rigidity-tuning conductive elastomer," *Smart Mater. Struct.*, vol. 24, no. 6, 2015, Art. no. 065001.
- [12] Z. Zhakypov, C. H. Belke, and J. Paik, "Tribot: A deployable, self-righting and multi-locomotive origami robot," in *Proc. IEEE/RSJ Int. Conf. Intell. Robots Syst.*, 2017, pp. 5580–5586.
- [13] J. Sun, B. Pawlowski, and J. Zhao, "Embedded and controllable shape morphing with twisted-and-coiled actuators," in *Proc. IEEE/RSJ Int. Conf. Intell. Robots Syst.*, 2018, pp. 5912–5917.
- [14] M. Manti, V. Cacciuoli, and M. Cianchetti, "Stiffening in soft robotics: A review of the state of the art," *IEEE Robot. Autom. Mag.*, vol. 23, no. 3, pp. 93–106, Sep. 2016.
- [15] T. L. Buckner, E. L. White, M. C. Yuen, R. A. Bilodeau, and R. K. Kramer, "A move-and-hold pneumatic actuator enabled by self-softening variable stiffness materials," in *Proc. IEEE/RSJ Int. Conf. Intell. Robots Syst.*, 2017, pp. 3728–3733.
- [16] A. Tonazzini, S. Mintchev, B. Schubert, B. Mazzolai, J. Shintake, and D. Floreano, "Variable stiffness fiber with self-healing capability," *Adv. Mater.*, vol. 28, no. 46, pp. 10142–10148, 2016.
- [17] M. Taghavi, T. Helps, B. Huang, and J. Rossiter, "3D-printed ready-to-use variable-stiffness structures," *IEEE Robot. Autom. Lett.*, vol. 3, no. 3, pp. 2402–2407, Jul. 2018.
- [18] L. L. Howell, *Compliant Mechanisms*. Hoboken, NJ, USA: Wiley, 2001.
- [19] M. C. Yuen, R. A. Bilodeau, and R. K. Kramer, "Active variable stiffness fibers for multifunctional robotic fabrics," *IEEE Robot. Autom. Lett.*, vol. 1, no. 2, pp. 708–715, Jul. 2016.
- [20] A. G. Erdman, G. N. Sandor, and S. Kota, *Mechanism Design: Analysis and Synthesis*, vol. 1. Englewood Cliffs, NJ, USA: Prentice-Hall, 1997.
- [21] L. L. Howell and A. Midha, "A method for the design of compliant mechanisms with small-length flexural pivots," *J. Mech. Des.*, vol. 116, no. 1, pp. 280–290, 1994.
- [22] H.-J. Su, "A pseudorigid-body 3R model for determining large deflection of cantilever beams subject to tip loads," *J. Mech. Robot.*, vol. 1, no. 2, 2009, Art. no. 021008.
- [23] D. E. Vogtmann, S. K. Gupta, and S. Bergbreiter, "Characterization and modeling of elastomeric joints in miniature compliant mechanisms," *J. Mech. Robot.*, vol. 5, no. 4, 2013, Art. no. 041017.
- [24] J. C. Klann, "Walking device," U.S. Patent 6478 314, Nov. 12 2002.
- [25] A. DeMario and J. Zhao, "Development and analysis of a three-dimensional printed miniature walking robot with soft joints and links," *J. Mech. Robot.*, vol. 10, no. 4, 2018, Art. no. 041005.
- [26] P. G. De Santos, E. Garcia, and J. Estremera, *Quadrupedal Locomotion: An Introduction to the Control of Four-Legged Robots*. New York, NY, USA: Springer, 2007.